

# Influence Factors of 3D Modeling with Aerial Images

Jwu-Jenq Chen<sup>1</sup>, Chieh-Ling Huang<sup>1\*</sup>, Yung-Gi Wu<sup>2</sup>, Po-Han Wu<sup>2</sup>

## ABSTRACT

Nowadays, UAV technology is mature and widely used in all aspects. UAV swarms can perform rather good performances than single UAV in aerial photography, images stitching and 3D modeling. In the integrated application of aerial photography, image stitching and modeling, the optimal overlap ratio of pairwise photos to facilitate image stitching and the best number of photos to facilitate modeling are important setting and research gaps. Therefore, this research takes photos by UAV swarm, calculates the overlap ratio and compares the effect of different overlap ratio on 3D modeling. In addition, this research compares the differences in modeling time, the number of feature points, and the number of feature points used for calibration. The result of experiment reveals that as the overlap rate of images increases, the processing time increases exponentially, but the increase in memory can only reduce the processing time linearly.

**Keywords:** image stitching; aerial images; overlap rate; 3D modeling; Point cloud

## I. INTRODUCTION

Unmanned aircraft vehicle (UAV) is also known as dynamic remotely operated navigation equipment (Drone). UAV was very unstable in the initial development. Nowadays, the technology UAV is mature and popular due to the development of UAV flight control computer that integrates with sensors and GPS by academic institution and industry. It makes the UAV become an airborne robot that can self-stabilize, return to launch point (RTL) automatically, integrate cameras or various devices and fly automatically according to missions setting in ground stations [1]. UAV has many advantages. The most obvious advantage is the safety of pilot just because there is no pilot onboard. Therefore, aerial photography can be taken over dangerous area and in lower attitude to avoid obscured by clouds. In

addition, the cost is much lower compare to the real aircraft with pilot. Due to the advantages of UAV mentioned above, it has many applications. Some of studies revealed that UAV widely utilized for numerous purposes, containing executing disaster rescue missions and monitoring wild fires [2-5]. It can deliver emergency supplies to inaccessible area. It can equip with thermal sensor to detect the effectiveness of solar panel [6]. It can also integrate camera to take pictures, and go a step further, join those pictures by overlay and construct 3D model.

As for the application of constructing 3D model by UAV, it can contribute to inference of the potential of soil-rock flow [7] and observe the condition of disaster. The Weiguan Building in Tainan collapsed at 3:57 am on February 6, 2016 caused by an earthquake occurred in southern Taiwan [8]. The laboratory of Digital City belonged to Department of Surveying and Spatial Information Science, National Cheng Kung University constructed the 3D model (as shown in Figure 1) by 177 aerial photos of 1200 pixels by DJI Phantom 3 Drone at 14:00 on February 7, 2016 [9] to assist in executing disaster rescue.

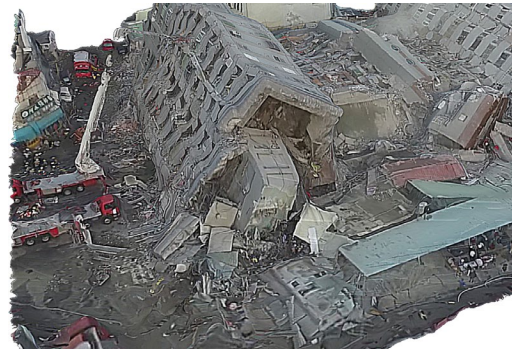


**Figure 1. The 3D model of the collapse of Weiguan Building**

The types of UAV include: aircraft UAV (figure2-a), helicopter UAV (figure2-b) and multicopter UAV (figure2-c). Each type of UAV has its advantages and disadvantages due to the different structures. The aircraft UAV is also known as fixed-wing aircraft UAV. It needs runway to take off and land. It also needs airspeed to avoid stalling. Therefore, aircraft UAV cannot hover in the air. On the other hand, helicopter UAV and multicopter UAV can take off and land without runway and can hover. The main difference between helicopter UAV and multicopter UAV is the duration of flight. The helicopter UAV has long

*\*Corresponding Author: Chieh-Ling Huang  
(E-mail:kaio@mail.cjcu.edu.tw)*

<sup>1</sup>*Department of Interactive Design, Chang Jung Christian University Tainan, Taiwan. No.1, Changda Rd., Gueiren District, Tainan City 71101, Taiwan.*

<sup>2</sup>*Department of Computer Science and Information Engineering, Chang Jung Christian University Tainan, Taiwan. No.1, Changda Rd., Gueiren District, Tainan City 71101, Taiwan.*

endurance than multicopter but the mechanical structure is complex. Due to the ability of hover and simple, multicopter UAV is much more popular than others and at this time, most aerial photos are taken from multicopter UAV. But multicopter's duration of flight is about only 15-20 minutes. This means that the area multicopter UAV can observe is small. Therefore, swarm of multicopter UAV can observe the double or treble area at one flight and clear the problem mentioned above [10].

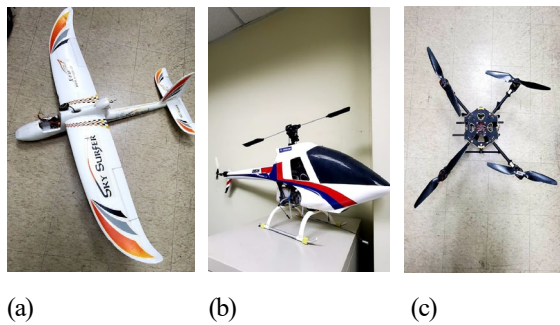


**Figure 2. Unmanned aircraft vehicle (UAV)**  
**(a) aircraft UAV (b) helicopter UAV (c) multicopter UAV**

After taking photos from single multicopter UAV or swarm, the image stitching is the important step for observing the large area or constructing 3D model. Nowadays, even mobile phone can stitch the images but the result is relatively rough. Usually, stitching of aerial photos needs a computer to process. The process is to input the image, capture and match the feature points from the overlap of two images, adjust the image such as light, shadow or angle, and finally join the image. The more overlap ratio of two images, the accuracy of stitching is higher but the area of those two images is smaller. For efficiency purposes, it is necessary to reveal the optimal overlap ratio of two images for stitching. Besides, this research reveals the optimal number of image for 3D modeling at the same time.

The structure of this paper is as follows: Section 2 describes the methods of taking aerial photos (single multicopter and swarm). Section 3 describes the related processing technology of image stitching; Section 4 introduces the modeling process of Pix4D software; Section 5 is the experimental results and discussion; Finally, Section 6 is the conclusion.

## II. METHODS OF TAKING AERIAL PHOTOS

Nowadays, most aerial photos are taken by a multicopter UAV at one time. Due to the limitation of flight duration and the regulations of attitude, usually, a multicopter UAV can fly 15 minutes and observe about the area of 200 m<sup>2</sup>. A multicopter UAV system includes a multicopter UAV and a

ground station. Multicopter UAV can be assembled by user. By using the Ardupilot software suite contributed by the Ardupilot development team and community, assembling a multicopter UAV system is no longer difficult. The hardware that Ardupilot software suite supported includes Pixhawk and Intel Aero etc. And the ground station controlling software Ardupilot software suite supported includes Mission Planner, APM Planner etc. The popular, open source ground station – “Mission Planner” has many functions including camera control and grid survey. The user can setup an aerial survey mission with path (as shown in Figure 3), front overlap and side overlap (as shown in Figure 4). Besides of assembling a multicopter system, there are some products available. For example, multicopter of DJI Phantom series with Pix4D App is one of the options. Pix4D App provides the functions with survey mission (as shown in Figure 5), front overlap and side overlap also (as shown in Figure 6).

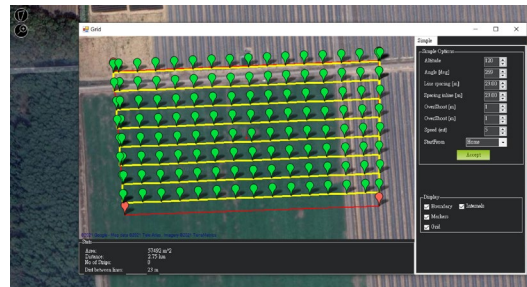


**Figure 3. Survey mission of Mission Planner**

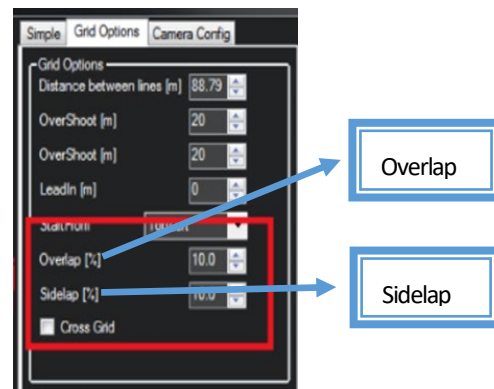


**Figure 4. Overlap setting of Mission Planner**



**Figure 5. Survey mission of Pix4D**

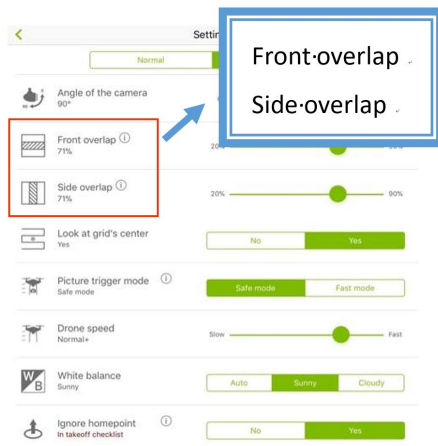


Figure 6. Overlap setting of Pix4D

Taking aerial photos can also be by UAV swarm. Although numerous researchers found that developing a swarm control system for UAV was feasible and plausible [11–17], the applications of UAV swarm focus on military and UAV swarm flying show [18-21]. In order to enlarge the aerial survey area by multicopter UAV during one flight, Chen etc., (2019) proposed a calculation method to make each UAV adjusts the distance automatically in order to make the areas of photos taken by every UAV connected or overlap according to the setting by user [10]. Base on the calculation method, this research constructed the multicopter UAV swarm system for aerial survey. In this system, Multi multicopter UAVs (follower UAV) follow up the leader multicopter UAV and adjust distances among UAVs automatically. The only thing the user need to do is setting up the flying path of the leader multicopter UAV, the other following multicopter UAV will follow the leader and adjust the distances according to lens and flight height (as shown in Figure 7).

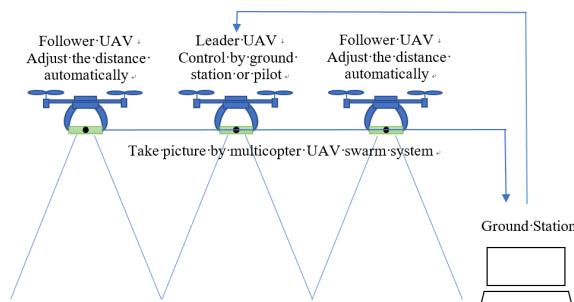


Figure 7. Multicopter swarm system

In order to make the follower multicopter UAVs adjust distances automatically, this research modified the open source ground station – “Mission Planner”. The swarm functions provided by mission planner contain “Swarm” and “Follow the Leader” (as shown in Figure 8). The function of “Swarm” makes UAVs fly in formation by setting the relative distances. But the distance can only be adjusted

manually, and cannot be changed in order to make the area of photos connected or overlap by setting. The function of “Follow the Leader” provides the user to specify a UAV as the leader and other UAVs will follow the leader UAV at a fixed distance [22]. Because those two functions cannot achieve the purpose of this research, modify the mission planner is necessary.

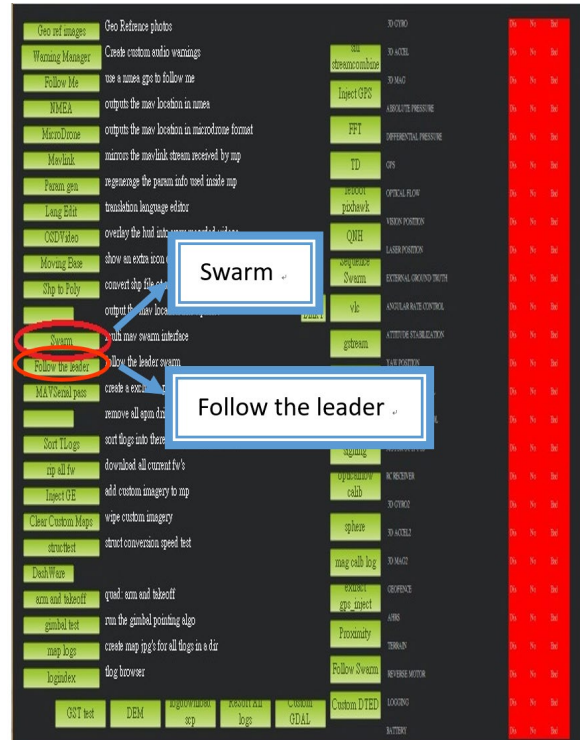


Figure 8. The functions of “Swam” and “Follow the Leader” of Mission Planner

The disadvantage of “Swarm” is the UAVs cannot adjust the distance between each other in order to make the area of photos connected or overlap by setting automatically. Therefore, this research rewrites the function of “Swarm”. In order to make the UAVs keep the distances automatically to make photos connected, the distance between the two UAVs should be [10]:

$$\text{Distance} = ((\text{CCD size}/2) / \text{focal length}) * \text{Altitude} * 2 \quad (1)$$

Therefore, the distance between each two UAVs can be calculated by equation 1 with the data of CCD size, focal length and flight height. This research rewrites the code of swarm as shown in figure 9 to make each UAV keeping the properly distance automatically.

```
double leadera = 10.583334, followera = 10.583334; // 底片尺寸
double leaderb = 27.8, followerb = 27.8; // 焦距
double shooting;
shooting = (leadera / 2 / leaderb * alt) + (followera / 2 / followerb * alt);
```

Figure 9. Code to adjust the distance of UAVs

Besides, the functions of “Horizontal Swarm Formation” and “Vertical Swarm Formation” are added by this research. There are three new buttons added by this research on the interface of swarm: “Horizontal Swarm Formation”, “Vertical Swarm Formation” and “Aerial Photography by Swarm” as shown in Figure 10.

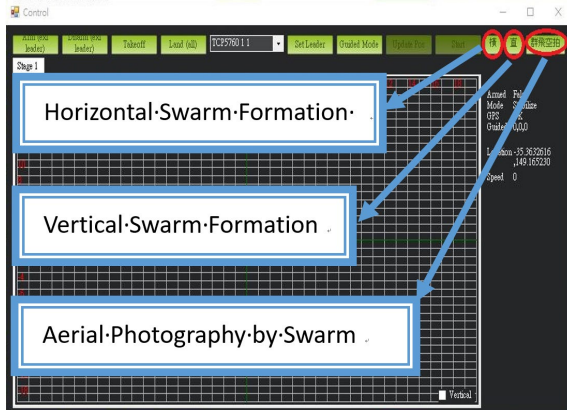


Figure 10. Interface of swarm with 3 new buttons

After taking off, the multicopter UAV pilot needs to control the leader multicopter UAV only and the follower UAVs follow the leader UAV horizontally or vertically automatically by clicking the buttons designed by this research (as shown in Figure 11). Once the function of “Aerial Photography by Swarm” is activated, the follower UAVs keep the distances automatically according to the camera lens and the flying height to make the aerial photography connected in order to have multiple range as shown in Figure 12.



Figure 11. UAVs keep the distance automatically



Figure 12. Aerial photography connected automatically

### III. PROCESSING OF IMAGE STITCHING

After taking the aerial photos by single multicopter or swarm, the next step is image stitching. In order to join those pictures by overlay, analyzing the mapping characteristics between two images is necessary, such as the corners and edges of the images. And then the image stitching is processed by those mapping characteristics.

#### 3.1 Corner Detection

##### 3.1.1. Moravec Corner Detector

Moravec corner detection algorithm [23] belongs to an early stage in the development of corner detection algorithms. Corner detection algorithm can detect the position of the corner in the image. Although Moravec corner detection algorithm has some disadvantages, it is the basis of many corner detection algorithms. The Harris corner detector that mentioned in the next paragraph is developed on the base of Moravec corner detector. The algorithm defines corner points as having low "autocorrelation". The algorithm detects each pixel of the image, uses neighborhood pixels around the pixel as a window, and detects the correlation between this window and other surrounding windows. This correlation is measured by the sum of squared differences (SSD) between two windows. The smaller the SSD, the higher the similarity. If the pixels are in the smooth image area, the surrounding windows will be very similar. If the pixel is on the edge, the surrounding windows will be very different in the direction orthogonal to the edge, and more similar in the direction parallel to the edge. If the pixel is a feature point that changes in all directions, all the surrounding windows will not be similar. Moravec will calculate the minimum SSD of each pixel window and surrounding windows as the intensity value, and take the point with the local maximum intensity as the feature point.

##### 3.1.2 Harris Corner Detector

The Harris algorithm [24] improves Moravec's method by considering the SSD of each pixel along a specific direction directly instead of calculating the SSD surrounding a pixel, so that it does not need to consume a lot of resources to calculate. And the result is not only the maximum value in the area, but also the corner point we want to find.

#### 3.2 Edge Detection

##### 3.2.1 Sobel algorithm

The Sobel edge detection algorithm [25] is a discrete difference operator used to calculate the approximate value of the gradient of the image brightness function. The disadvantage is that the Sobel algorithm does not separate the subject of the image from the background very well. In other words, the Sobel algorithm does not process the image based on the gray level. Because the Sobel algorithm does not simulate the physiological characteristics of human visual, the extracted image contour is sometimes unsatisfactory.

### 3.2.2 Canny algorithm

Canny edge detection algorithm [26] has more advantages than others, but it is more complicated to implement. The Canny algorithm is a multi-stage optimization operator with filtered and enhanced detection. Before processing, the Canny algorithm uses a Gaussian smoothing filter to smooth the image and remove noise. The Canny segmentation algorithm uses a finite first-order partial difference to calculate the gradient magnitude and direction. And then non-maximum suppression is processed. Finally, Canny algorithm uses two thresholds to connect the edges. It can detect the edges and points on the edges of the image effectively and the error of positioning is very small. However, it is more difficult to detect the features of people and complex images. Therefore, the Canny detection method may be more suitable for aerial images.

### 3.3 Feature point matching

After the feature points are captured, the feature points between the two images can be matched. At the same time, the overlap between the two images can be calculated, and then an overlap rate can be obtained for the following steps.

#### 3.3.1 RANSAC algorithm

The RANSAC algorithm [27] first uses a set of image transformation parameters randomly corresponding to the minimum estimation function, and extracts the minimum point set of  $n$  times to estimate the initial value of the parameter in the function iteratively. The initial value divides all data into in-groups and outliers. Finally, in turn, use all the in-groups to recalculate and estimate the parameters of the function.

$$1 - p = (1 - u^m)^n \quad (2)$$

$$N = \log(1 - p) / \log(1 - (1 - v)^m) \quad (3)$$

In the formula,  $p$  is the correct probability,  $u$  is the probability that the inner group appears in the data,  $v = 1 - u$  is the value of the outlier,  $N$  is the number of iterations, and  $m$  is the necessary number of point sets.

#### 3.3.2 Best Neighbor Matching Method

The first step of best neighbor matching method is finding a compatible homographic matrix  $H$  between a group of images by RANSAC, and then use a probability model to verify the match. RANSAC uses a set of image transformation parameters randomly corresponding to the minimum estimation function, and extracts the minimum point set of  $n$  times to estimate the initial value of the parameter in the function repeatedly. The initial value divides all data into in-groups and outliers. Finally, the parameters of the function are recalculated and estimated by all inner groups.

$$p(H \text{ is correct}) = 1 - (1 - (p_i)^n)^n \quad (4)$$

In the formula,  $p$  is the correct probability,  $n$  is the number of iterations,  $p_i$  is the probability that the inner group

appears in the data, and  $r$  is the number of feature corresponding points.

#### 3.3.3 SURF feature point matching

The SURF algorithm [28] is improved from the SIFT algorithm [29]. SIFT uses continuous Gaussian filters of different scales to process the image, and uses Gaussian difference to detect feature points in the image. SURF uses a square filter to achieve Gaussian blur approximation. The OpenCV library of image processing can be used for feature point detection and matching of the SURF algorithm.

After the image is matched with the feature points through the SURF algorithm, several groups of feature points are selected by random. And then the error distance of the corresponding point is calculated by the root mean square of each feature point. Finally, the two points with smallest error distance are used for geometric transformation of the image and then joined.

## IV. CONSTRUCTING 3D MODEL

Pix4D software (Pix4Dmapper) is a professional software of aerial telemetry. It can process aerial, tilt and ground images captured by any camera. Its output of Pix4D is applicable to various industries with the accuracy of the meter level and the three-dimensional accuracy like LiDAR. All calibrations are automatically completed, and the results are available for immediate use. It can produce high-resolution orthoimages, point clouds, numerical surface models, contour lines, etc., and provide functions such as drawing 3D line segments, labeling objects, and calculating volume. The software can be downloaded from official website [11]. The download page is shown as Figure 13.

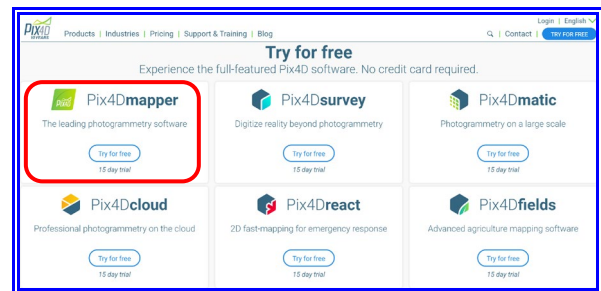


Figure 13 Download page of Pix4D

This research uses this software to construct 3D model from 2D aerial images, and furthermore, finds out the effects of different aerial image overlap ratios on 3D modeling by Pix4D. These effects that this research revealed are not only the completeness of the 3D model, but also include the comparison of the modeling time, the number of feature points, and the number of feature points used for correction. The purpose is to find a suitable overlap rate with better model integrity and modeling time.

The process of Pix4D to create a 3D model from 2D images is shown in Figure 14. The entire process includes four steps: (1) creating a project, (2) importing aerial images,

(3) parameter settings, and (4) modeling calculations. The detailed software instructions are as follows:

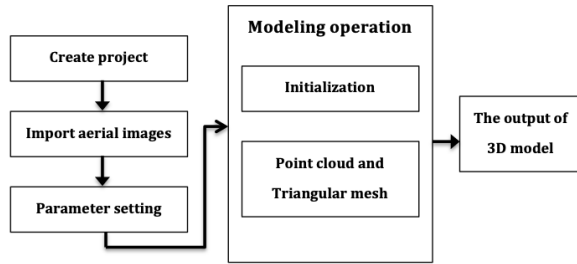


Figure 14 Process of Pix4D to create a 3D model

(1) Create project

Run the Pix4D software, and the function of creating new project will appear as shown in Figure 15.



Figure 15 Function of creating new project of Pix4D

(2) Import aerial images

The function of importing aerial images into the project is shown in Figure 16.



Figure 16 The function of importing images of Pix4D

(3) Parameter setting

The parameter setting includes camera model parameters, image location, options of constructing 3D map or 3D model.

(4) Modeling operation

The modeling operation includes two steps: (a) initialization and (b) point cloud and triangular mesh.

The initialization step process the estimation of point cloud. In this step, the point cloud position represented by the

feature points is calculated from the feature points between the images, and then inference the location where the images were taken. Figure 17 shows the point cloud estimated by Pix4D and the locations where the images were taken inferred from point cloud. It can be seen from Figure 17 that the estimated point cloud is not dense. Therefore, point cloud densification and triangular mesh are produced in the next step. Figure 18(a) is the result of point cloud densification and 18(b) is the result of the triangular mesh.

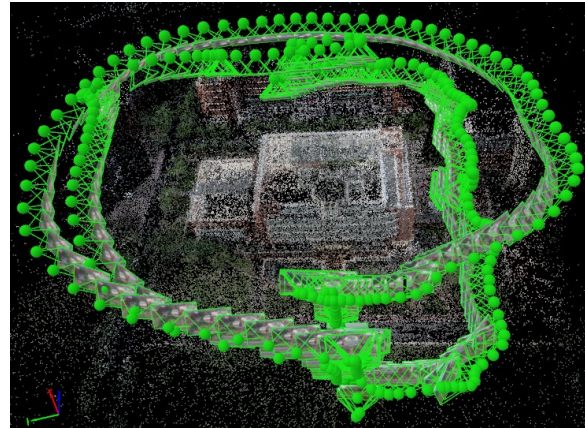


Figure 17 Point cloud and the locations where the images were taken

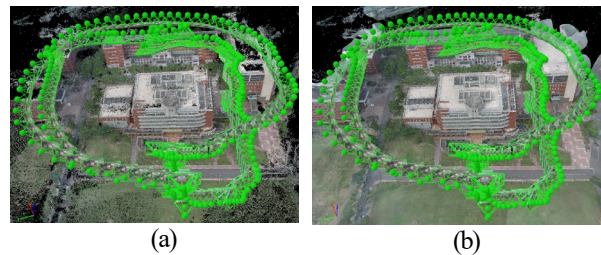


Figure 18 Pix4D

(a) Point cloud densification (b) Triangular mesh

## V. EXPERIMENT AND ANALYSIS

In the implementation of image stitching in this research, Visual Studio 2015 is used as the development environment, combined with the contents of the OpenCV library to implement image stitching.

### 5.1 The Result of Corner Detection

#### 5.1.1 Moravec corner detection

Figure 19(a) is the original image of corner detection. The corner points found in Figure 19(b) are not obvious and the number is very rare. However, if the original image is a box as shown in Figure 20(a), the corner points can be found accurately as shown in Figure 20(b).



**Figure 19 The result of Moravec corner detection I**  
 (a) Original image (b) The result of corner detection

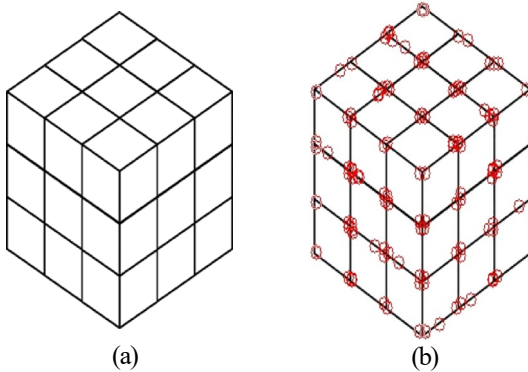


**Figure 20 The result of Moravec corner detection II**  
 (a) Original image (b) The result of corner detection

### 5.1.2. Harris corner detection

Harris corner detection can find the corners accurately. Figure 21(a) is the original image. It is obviously that the result of Harris corner detection by OpenCV 3.0 library as shown in Figure 21(c) is more accuracy than the result by OpenCV 2.4 library as shown in Figure 21(b).

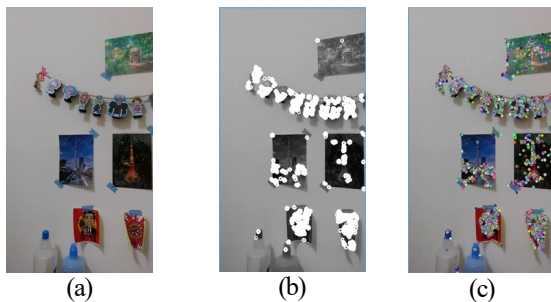


**Figure 21. The result of Harris corner detection**  
 (a) Original image (b) The result of OpenCV 2.4 (c) The result of OpenCV 3.0

## 5.2 The Result of Edge detection

### 5.2.1 Sobel edge detection

The result of Sobel edge detection is good (as shown in Figure 22), but some edges are blurred.

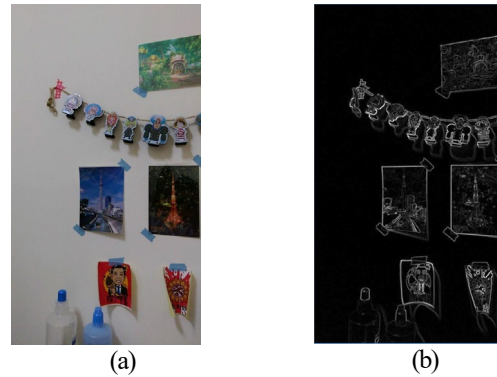


**Figure 22 The result of Sobel edge detection**  
 (a) Original image (b) The result of edge detection

### 5.2.2 Canny edge detection

The result of Canny edge detection is good. As shown in Figure 23, the edges of venetian blinds are detected correctly.



**Figure 23 The result of Canny edge detection**  
 (a) Original image (b) The result of edge detection

## 5.3 The Result of Image Stitching

Two images are used for image stitching (as shown in Figure 24). Figure 25 is the stitching result by the library of OpenCV 2.4 and Figure 26 is the result by SURF algorithm.



**Figure 24 Original images for stitching**



**Figure 25 Image stitching by the library of OpenCV 2.4**



Figure 26 Image stitching by SURF algorithm.

The result in Figure 25 is very good, but part of the image will be cut off. However, the stitching result of the SURF algorithm in Figure 26 is not as satisfactory as the result in Figure 25, but it can maintain most of the image to facilitate the calculation of the image overlap rate after stitching.

### 5.4 The effect of image overlap rate on 3D modeling

For the calculation of estimating 3D point cloud from 2D image by Pix4D software, the equipment used in this research is DELL T410 server. DELL T410 server is equipped with 2 Intel Xeon CPU X5650, with a total of 12 cores (24 threads). Its CPU frequency is 2.67 Ghz, and is equipped with 34G DDR3 ECC REG RAM. The aerial images for experiment are divided into 8 data sets according to different image overlap rates. The number of aerial images in each set and the calibration adoption rate are shown in Table 1.

Table 1 The number of aerial images in each group and the calibration adoption rate

| # | N.I. | O.R.  | P.E.E.T.    | NDI | NCI  | CAR   |
|---|------|-------|-------------|-----|------|-------|
| 1 | 21   | 27.19 | 31s         | 0   | 9    | 42.86 |
| 2 | 105  | 80.68 | 06m:46s     | 1   | 104  | 100   |
| 3 | 210  | 85.56 | 29m:10s     | 1   | 209  | 100   |
| 4 | 420  | 94.95 | 01h:32m:46s | 15  | 405  | 100   |
| 5 | 600  | 96.93 | 02h:13m:47s | 45  | 555  | 100   |
| 6 | 840  | 97.76 | 06h:21m:09s | 91  | 749  | 100   |
| 7 | 1007 | 98.54 | 07h:15m:22s | 139 | 868  | 100   |
| 8 | 1798 | 99.38 | 24h:40m:11s | 401 | 1397 | 100   |

N.I.: Number of images; O.R.: Overlap ratio(%);  
 P.C.E.T.: The point cloud estimation time;  
 N.D.I.: The number of disabled images  
 N.C.I.: The number of calibration images  
 C.A.R.: The calibration adoption rate(%)

The overlap ratio (O.R.) in Table 1 is the overlap ratio between the images. The point cloud estimation (P.C.E.T) time is the time spent in the first step to initialize the point cloud estimation. The number of disabled images (N.D.I) is the number of images that the Pix4D software is not used to estimate the point cloud. The number of calibration images (N.C.I) is the number of images used to be calibrated; and the calibration adoption rate (C.A.R.) is the percentage of the image used for correction in the point cloud image estimated by the Pix4D software.

It can be found from Table 1 that when the image overlap rate is too low, such as the #1 data sets, the calibration adoption rate will be low as well, and the accuracy

of modeling will be relatively unreliable. When the image overlap rate is too high, the system also makes the number of disabled images increase relatively in order to reduce the amount of repeated calculations. The relationship between the number of images and processing time of the point cloud is shown in Figure 27. It appears that the relationship between the processing time and the number of images is exponential relationship.

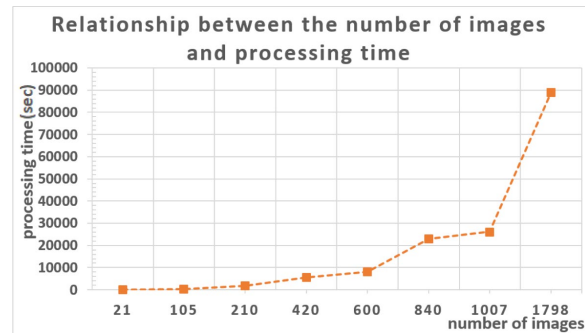


Figure 27 Relationship between the number of images and processing time of the point cloud

Table 2 and Table 3 show the number of corresponding feature points between images and the number of feature points used for calibration. Since the aerial images used are in the same group, the number of corresponding feature points calculated from each group of data is very similar; and the number of feature points used for calibration tends to be proportional to the overlap rate. The increase in the number of calibrated feature points helps to improve the accuracy of point cloud estimation.

Table 2 the number of corresponding feature points

| # | N.I. | O.R.   | Number of corresponding feature points |      |      |      |
|---|------|--------|--|------|------|------|
|   |      |        | Median                                 | Max  | Min  | Mean |
| 1 | 21   | 27.19% | 7841                                   | 7415 | 8172 | 7796 |
| 2 | 105  | 80.68% | 7448                                   | 6678 | 8920 | 7480 |
| 3 | 210  | 85.56% | 7441                                   | 6490 | 8920 | 7481 |
| 4 | 420  | 94.95% | 7431                                   | 6490 | 8920 | 7478 |
| 5 | 600  | 96.93% | 7397                                   | 6555 | 9970 | 7467 |
| 6 | 840  | 97.76% | 7416                                   | 6490 | 8920 | 7466 |
| 7 | 1007 | 98.54% | 7416                                   | 6540 | 9004 | 7467 |
| 8 | 1798 | 99.38% | 7455                                   | 6555 | 9970 | 7490 |

N.I.: Number of images; O.R.: Overlap ratio(%)

Table3 the number of feature points used for calibration

| # | N.I. | O.R.   | Number of corresponding feature points |      |      |         |
|---|------|--------|--|------|------|---------|
|   |      |        | Median                                 | Max  | Min  | Mean    |
| 1 | 21   | 27.19% | 1821                                   | 130  | 3872 | 2102.83 |
| 2 | 105  | 80.68% | 3605                                   | 447  | 5857 | 3625.82 |
| 3 | 210  | 85.56% | 4102                                   | 712  | 6014 | 4048.67 |
| 4 | 420  | 94.95% | 4312                                   | 974  | 5806 | 4286.09 |
| 5 | 600  | 96.93% | 4288                                   | 1097 | 5697 | 4351.86 |
| 6 | 840  | 97.76% | 4255                                   | 848  | 5636 | 4331.66 |
| 7 | 1007 | 98.54% | 4221                                   | 1378 | 5592 | 4296.18 |
| 8 | 1798 | 99.38% | 4090                                   | 1614 | 5478 | 4185.58 |

N.I.: Number of images; O.R.: Overlap ratio(%)

This research takes the 3D models that constructed from six sets of aerial image (#1, #2, #3, #4, #6, and #7) for comparison. Figure 28 shows the point cloud and camera position calculated by Pix4D. Due to the low overlap rate of #1, the number of point clouds established is lower than others. As shown in Figure 28(a), the established point clouds are extremely sparse. This phenomenon can be improved by densifying the point cloud and building triangular mesh in the second step.

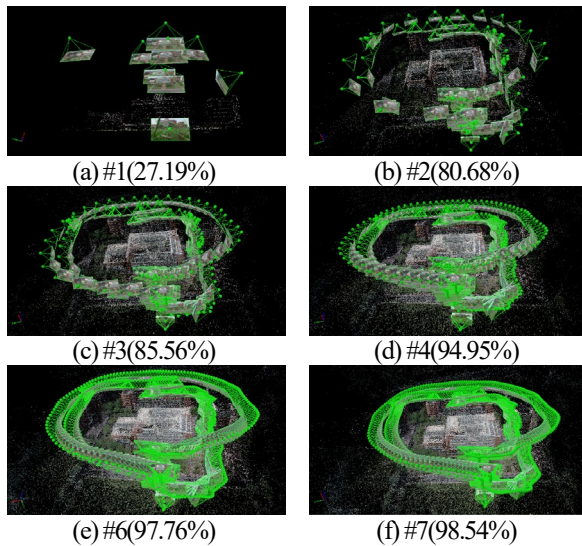


Figure 28 The point cloud and camera position

The result of 3D models constructed by the triangular mesh are shown in Figure 29. In this step, the six sets of aerial image (#1, #2, #3, #4, #6, and #7) are used for building triangular mesh. The 3D model constructed from #1 is not in its integrity due to the the lower overlap rate of aerial images as shown in Figure 19(a). The other five 3D models constructed from the sets of aerial images (#2, #3, #4, #6, #7) are almost the same and difficult to distinguish the differences.

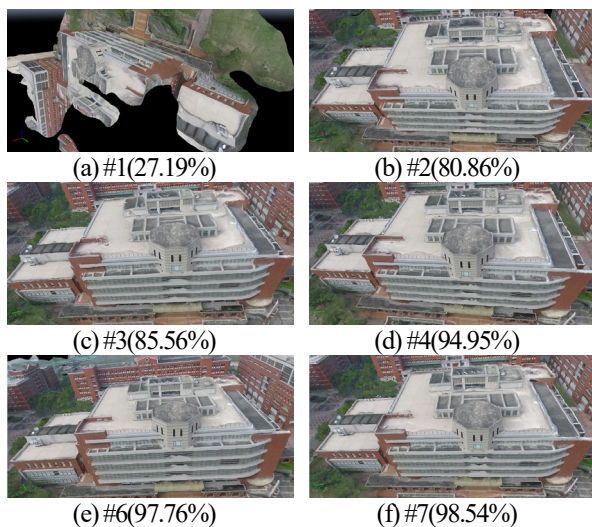


Figure 29 3D models constructed by the triangular mesh

Finally, this research observed the difference of processing time by increased the memory from 34G to 98G. Table 4 shows the information of processing time. It is obvious that the processing time can be reduced by increasing the memory. The speed increases to 215% when the memory increases to 288% (Min: 137%~ Max: 283%).

Table 4 The processing time and memory

| # | N.I. | Processing time |        | # | N.I. | Processing time |           |
|---|------|-----------------|--------|---|------|-----------------|-----------|
|   |      | 34G             | 98G    |   |      | 34G             | 98G       |
| 1 | 21   | 31"             | 17"    | 5 | 600  | 2:13'47"        | 1:2'37"   |
| 2 | 105  | 06:46"          | 4'57"  | 6 | 840  | 6:21'09"        | 2:19'33"  |
| 3 | 210  | 29:10"          | 13'47" | 7 | 1007 | 7:15'22"        | 2:50'59"  |
| 4 | 420  | 1:32'46"        | 38'28" | 8 | 1798 | 24:40'11"       | 10:35'27" |

N.I.: Number of images

## VI. CONCLUSIONS

This research discusses the effect of 2D image overlap rate obtained by aerial photography on 3D modeling. Besides, the related methods of taking aerial photography and image stitching are discussed and implemented to facilitate the calculation and setting of image overlap rate. The methods of taking aerial photography including single multicopter UAV and swarm are implemented and compared. The methods of image stitching including: corner detection, edge detection, and the algorithms of feature point matching are implemented and discussed too. The effect of 2D image overlap rate on 3D modeling is also fully discussed and quantitative analysis in the experimental results. This study found that as the overlap rate increases, the processing time also increases exponentially, but increasing memory can only reduce the processing time linearly.

## ACKNOWLEDGMENTS

This work was supported by Minister of Science and Technology of the Republic of China under contract number MOST 109-2221-E-309-002.

## REFERENCES

- [1] C.C. Liu, J. J. Chen, "Research on Service Quality Criteria for UAV Filming and Photography in Taiwan-Dual Perspective", International Journal of Applied Business and Economic Research, Vol. 15, No 15, pp. 101-121, Aug. 2017.
- [2] C. C. Pai, Y. C. Liu, Y. S. Hsiao, H. P. Lien and P. H. Lin, "Analysis of Accuracy for UAV-derived Topography from a GoPro Camera", Journal of Chinese Soil and Water Conservation. Vol. 46, pp. 142-149, 2015.
- [3] J. Y. Rau, C. Y. Chen, J. P. Jhan, K. Liu and W. Lee, "Accuracy Analyses of UAV Photogrammetry and Direct Georeferencing", Taiwan Journal of Geoinformatics, vol. 2, pp. 1-22, 2013.

- [4] W. Chang, Y. S. Hsiao, and J. C. Chang, "Feasibility Analyses of River Sediment Estimation and Mountain Mapping by UAV Techniques", *Journal of Chinese Soil and Water Conservation*, Vol. 48, pp. 1-13, 2017.
- [5] S. H. Chio, "Accuracy Elevation of Orthoimages for Aviation Occurrence Site from Rotary UAS Images", *Journal of Aviation Safety and Management*. Vol. 2, pp. 400-417, 2015.
- [6] C. L. Lin, J. J. Chen, S. L. Chuang, Y. Li and C. S. Chou, "The Efficiency Evaluated System for Solar Panel by Drone with Infrared Sensor", *International Conference of Computational Methods in Sciences and Engineering 2018 (ICCMSE 2018)*, Greece, Mar. 2018.
- [7] U. Niethammer, M.R. James, S. Rothmund, J. Travelletti, and M. Joswig, "UAV-based remote sensing of the Super-Sauze landslide: Evaluation and results", *Engineering Geology*, Vol. 128, pp. 2-11, March 2012.
- [8] <http://scweb.cwb.gov.tw/GraphicContent.aspx?ItemId=49&fileString=2016020603572666006>, accessed March 2020.
- [9] <http://sketchfab.com/3d-models/e1afea999b534dd6bcc1fde663f3e7ed>, accessed March 2020.
- [10] J. J. Chen, Y. G. Wu and C. L. Lin, "Applying Distance Maintaining Calculation Method on Multi-rotor UAV Swarm", *International Conference of Computational Methods in Sciences and Engineering (ICCMSE 2019)*, Rhodes, May. 2019.
- [11] <http://www.defenceprocurementinternational.com/features/air/drone-swarms>, accessed March 2020.
- [12] A. G. Madey, "Unmanned Aerial Vehicle Swarms: The Design and Evaluation of Command and Control Strategies using Agent-Based Modeling", *International Journal of Agent Technologies and Systems*, Vol. 5, pp. 1-13, 2013.
- [13] <https://thediplomat.com/2018/02/chinas-swarms-of-smart-drones-have-enormous-military-potential>, accessed March 2020.
- [14] P. Vincent and I. Rubin, "A framework and analysis for cooperative search using UAV swarms", *ACM Symposium on Applied Computing*, New York, 2004.
- [15] R. J. Bamberger, D. P. Watson, D. H. Scheidt and K. L. Moore, "Flight Demonstrations of Unmanned Aerial Vehicle Swarming Concepts", *Johns Hopkins APL Technical Digest*, Vol. 27, pp. 41-55, 2006.
- [16] P. Dasgupta, "A Multiagent Swarming System for Distributed Automatic Target Recognition Using Unmanned Aerial Vehicles", *IEEE Transactions on Systems, Man, and Cybernetics - Part A: Systems and Humans*, Vol. 38, pp. 549-563, 2008.
- [17] A. Bandala, E. P. Dadios, R. R. P. Vicerra and L. A. G. Lim, "Swarming Algorithm for Unmanned Aerial Vehicle (UAV) Quadrotors: Swarm Behavior for Aggregation, Foraging, Formation, and Tracking", *Journal of Advanced Computational Intelligence and Intelligent Informatics*, Vol. 18, pp. 745-751, 2014.
- [18] <http://www.auvsi.org/industry-news/teams-swarm-systems-integrators-develop-uas-swarm-infrastructure-us-military>, accessed March 2020.
- [19] J. Packer, and J. Reeves, "Romancing the Drone: Military Desire and Anthropophobia from SAGE to Swarm," *Canadian Journal of Communication*, Vol. 38, pp. 309-331, 2013.
- [20] <http://www.cnn.com/2018/07/17/intel-breaks-world-record-2018-drones.html>, accessed March 2020.
- [21] <http://www.bloomberg.com/news/articles/2017-02-07/1-ady-gaga-s-halftime-drone-swarm-was-pretaped-to-shield-crowd>, accessed March 2020.
- [22] <http://ardupilot.org/planner/>, accessed March 2020.
- [23] H. Moravec, "Obstacle Avoidance and Navigation in the Real World by a Seeing Robot Rover", tech. report CMU-RI-TR-80-03, Robotics Institute, Carnegie Mellon University & doctoral dissertation, Stanford University, Sept. 1980.
- [24] C. Harris and M. Stephens, "A combined corner and edge detector", *Alvey Vision Conference*, pp. 147-151, 1988.
- [25] I. Sobel, and G. Feldman, "A 3x3 Isotropic Gradient Operator for Image Processing", presented at a talk at the Stanford Artificial Project, 1968.
- [26] J. Canny, "A computational approach to edge detection", *IEEE Trans. Pattern Anal. Machine Intelligence*, Vol. 8, No. 6, pp. 679-698, 1986.
- [27] A. Martin, Fischler, and R. C. Bolles. "Random Sample Consensus: A Paradigm for Model Fitting with Applications to Image Analysis and Automated Cartography", *Comm. of the ACM*, vol. 24, no. 6, pp. 381-395, June 1981.
- [28] B. Herbert, E. Andreas, T. Tinne, and V. G. Luc, "SURF: Speeded Up Robust Features," *Computer Vision and Image Understanding (CVIU)*, Vol. 110, No. 3, pp. 346-359, 2008.
- [29] Lowe, and G. David, "Object recognition from local scaleinvariant features", *Proc. of the International Conference on Computer Vision*, pp. 1150-1157, 1999.



**Jwu-Jenq Chen** received the MS in Computer Science from Ohio University, U.S.A., 1996, and Ph.D. in Business and Operations Management from Chang Jung Christian University (CJCU), Taiwan, in 2018. He is currently an assistant Professor at the Department of Interactive Design, Chang Jung Christian University (CJCU). His current research interests are UAV system, Computer Vision, Decision Making, and Strategic analysis. He is a member of Phi Tau Phi honor society.



**Chieh-Ling Huang** received the BS in Electrical Engineering from National Taiwan University of Science and Technology (NTUST), Taiwan, in 1998, and the MS and Ph.D. in Electrical Engineering from National Cheng Kung University (NCKU), Taiwan, in 2000 and 2008, respectively. He is currently an Associate Professor and chairman at the Department of Interactive Design, Chang Jung Christian University (CJCU). His current research interests are Extended Reality technology, Somatosensory Interaction, Image Processing, Video Image Analysis, RFID (Radio Frequency Identification) technology and Wireless Sensor Network. He is a member of Phi Tau Phi honor society.



**Yung-Gi Wu** received his BS in the Department of Information & Computer Engineering, Chung Yuan Christian University, Taoyuan, Taiwan, 1992. He received his MS and Ph. D. degrees from the Institute of Electrical Engineering, National Cheng Kung University, Tainan,

Taiwan in 1994 and 2000, respectively. From 1994 to 1996, he was as a ROTC officer in military. He became an assistant professor and associate professor in 2000 and 2003. He is now a professor with the Department of Computer Science & Information Engineering, Chang Jung Christian University, Taiwan. His research fields include data compression, optimization, information retrieval, digital signal processing, intelligent emotion system design.



**Po-Han Wu** received the BS in Department of Computer Science and Information Engineering from Chang Jung Christian University (CJCU), Taiwan, in 2014, and the MS in Department of Computer Science and Information Engineering from Chang Jung Christian University (CJCU),

Taiwan in 2016. He currently works at Epileds. His current research interests are Image Processing, Video Image Analysis.